PHYSICAL REVIEW B **108**, 165417 (2023)

Crystalline membranes under stress: A Monte Carlo study based on the Nelson-Peliti Hamiltonian

R. Ramírez,[1,*] P. Tarazona,[2] E. Chacón,[1] and C. P. Herrero[1]

[1]*Instituto de Ciencia de Materiales de Madrid (ICMM), Consejo Superior de Investigaciones Científicas (CSIC), Campus de Cantoblanco, 28049 Madrid, Spain*

[2]*Departamento de Física Teórica de la Materia Condensada, Condensed Matter Physics Center (IFIMAC) and Instituto de Ciencia de Materiales Nicolas Cabrera, Universidad Autónoma de Madrid, 28049 Madrid, Spain*

(Received 9 June 2023; accepted 11 October 2023; published 20 October 2023)

A Monte Carlo study of a crystalline membrane described by the Nelson-Peliti Hamiltonian is presented. The membrane is studied for vanishing in-plane strain, as well as in the presence of tensile biaxial strain. The equilibrium simulations are performed in the classical limit as a function of temperature and system size, with elastic constants appropriate to the description of graphene. In the long-wavelength limit, the out-of-plane fluctuations of the unstrained membrane are described by a nonanalytic function with a critical exponent $\eta = 0.8$, in agreement with previous results based on the Nelson-Peliti Hamiltonian. Isotherm curves in the stress-strain plane allow us to identify the region of thermodynamic stability of the flat membrane. The most striking result is that the flat unstrained membrane, as described by the Nelson-Peliti Hamiltonian, is thermodynamically unstable at any finite temperature. A critical tensile biaxial stress is needed to reach the region of thermodynamic stability of the flat membrane. The critical strain is a monotonically increasing function of temperature. At any given temperature, the critical strain corresponds to the state with a minimum value of the real area of the membrane.

DOI: 10.1103/PhysRevB.108.165417

I. INTRODUCTION

Thermal fluctuations of crystalline membranes were studied in 1987 by Nelson and Peliti showing that they differ noticeably from their fluid counterparts [1]. These authors presented an effective elastic Hamiltonian that describes the anharmonic coupling between out-of-plane and in-plane membrane fluctuations. Their main result was that the effective bending rigidity of the out-of-plane fluctuations increases in the long-wavelength limit. This anharmonic effect favors a planar morphology of the crystalline membrane, as opposed to a crumpled one [2]. The discovery of graphene and other two-dimensional (2D) crystalline membranes has boosted the interest in understanding the anharmonic effects that are responsible for the intrinsic thermal rippling and the stability of the flat morphology of these sheets [3,4].

The anharmonic character of the Nelson-Peliti Hamiltonian prevents the derivation of its exact solution. Therefore several approximate methods have been developed so far. The result of these approximations can be expressed by the relationship between the amplitude of the out-of-plane fluctuations $|A_q|^2$, and their inverse wavelength ($q \propto \lambda^{-1}$) in the long-wavelength limit $q \rightarrow 0$ ($\lambda \rightarrow \infty$). The simple self-consistent approximation presented by Nelson and Peliti [1] predicts a power-law relation $|A_q|^2 \propto q^{\eta-4}$ with $\eta = 1$. An alternative presentation of this result is to consider that the flat membrane has an effective bending modulus of rigidity $\kappa(q) \propto q^{-\eta}$ in the long-wavelength limit. The larger the value of the positive exponent η, the lower the amplitude of the out-of-plane fluctuations, and the larger the rigidity and accordingly the stability of the flat membrane. Approximations based on classical first-order perturbation theory predict an exponent $\eta = 2$ [5]. However, Ahmadpoor *et al.* using variational perturbation theory obtain also a power-law behavior but with an exponent $\eta = 1$ [6].

There seems to be a general agreement that the most accurate approximations of the Nelson-Peliti model are provided by the self-consistent screening approximation (SCSA) and by renormalization group (RG) methods [7]. Le Doussal and Radzihovski using the SCSA found that the fluctuations of a tensionless membrane are determined by a critical exponent $\eta = 0.821$ [8,9]. A nonperturbative RG method found a similar value, $\eta = 0.849$ [10,11], while a recent RG approach using methods of perturbative field-theoretical renormalization reports $\eta = 0.795$ [12].

An alternative to variational, perturbative, and RG approaches is to study the Nelson-Peliti Hamiltonian by computer simulations. A Monte Carlo (MC) simulation of a crystalline membrane using this Hamiltonian was presented by Tröster [13,14]. This author aims at a numerical estimate of the critical exponent that challenges those previously derived by other methods, claiming an unprecedented accuracy in his algorithm. His numerical estimate of the critical exponent is $\eta = 0.795$.

Atomistic simulations using empirical interatomic potentials to describe elastic properties, as opposed to the elastic continuum approaches, have been performed to study anharmonic effects in graphene. A MC simulation with $\sim 4 \times 10^4$ atoms using the LCBOPII potential reports an asymptotic behavior of the out-of-plane fluctuations that seems to be described by a critical exponent $\eta = 0.85$ [15]. Another MC

---

[*] ramirez@icmm.csic.es

simulation of graphene using a Tersoff potential and including $\sim 10^5$ atoms reports an exponent $\eta \sim 0.85-0.88$ [16]. In the comparison of these MC results with the expectations of the Nelson-Peliti Hamiltonian, one should realize that these simulations were performed using realistic interatomic models, i.e., not a simpler elastic Hamiltonian, and that the relatively small size of the simulation cells makes less reliable the extrapolation to the asymptotic behavior in the thermodynamic limit.

The application of finite tensile strain to the projected area of a membrane has been considered previously by the SCSA with the Nelson-Peliti Hamiltonian [17]. The main result is that the anharmonic effects described by a critical exponent are suppressed in the long-wavelength limit, thus finding that $|A_q|^2 \propto q^{-2}$. Similar results were derived later using variational perturbation theory by Ahmadpoor *et al.* [6]. These authors present a lucid derivation of the statistical mechanics of the nonlinear elasticity described by the Nelson-Peliti Hamiltonian, in the presence of external uniform biaxial strain, which we have found useful for our present paper.

We aim to extend previous MC simulations of an unstrained crystalline membrane using the Nelson-Peliti Hamiltonian [13,14] to the case that the membrane is subject to an external uniform biaxial strain. Stress, the thermodynamic variable conjugate to the projected area, is then explicitly treated in the simulations. In addition to the spectrum of out-of-plane fluctuations as a function of stress, temperature, and system size, the isothermal stress-strain curves of the crystalline membrane are analyzed here. Our results allow us to identify the region of thermodynamic stability of the flat crystalline membrane. At finite temperature, the unstrained planar membrane, whose spectrum of out-of-plane fluctuations is determined by the critical exponent η, is shown to be thermodynamically unstable. This result is relevant to our present understanding of the anharmonic effects that are responsible for the thermal stability of the planar morphology of graphene and other solid membranes.

The paper is organized as follows. The Nelson-Peliti Hamiltonian is introduced in Sec. II. The setup of our MC simulations is explained in Sec. III. The results are presented in Sec. IV, which is divided into several subsections. An analysis of the elastic energy using the virial theorem is discussed in Sec. IV A. The partition of the elastic energy into mode dependent contributions as a function of the applied strain is presented in Sec. IV B. The amplitudes of the out-of-plane fluctuations, as derived from the MC simulations, are discussed in Sec. IV C. Numerical fits to these amplitudes are studied in Sec. IV D. Finite-size effects of the unstrained membrane are quantified in Sec. IV E. Isothermal stress-strain curves are presented in Sec. IV F, while the region of thermodynamic stability of the flat membrane is studied in Sec. IV G. The role of the real area in the thermodynamic stability of the crystalline membrane is discussed in Sec. IV H. The influence of selected anharmonic effects on the stability of the flat morphology of the crystalline membrane is analyzed in Sec. IV I. The paper closes with a summary.

II. NELSON-PELITI HAMILTONIAN

The Nelson-Peliti Hamiltonian describes the elastic properties of a flat membrane with crystalline order [1]. In this section this Hamiltonian is presented following closely Ref. [6]. The three following subsections introduce: (i) basic variables employed in real and reciprocal space; (ii) the effective elastic energy; and (iii) the calculation of the membrane stress.

A. Strain tensor and the spectrum of out-of-plane amplitudes

Let us consider a flat membrane with equilibrium position in the (x, y) plane, $\mathbf{R}_0 = (x, y, 0)$. After an elastic deformation, the new position vectors are denoted by $\mathbf{R}$. The displacement vectors $\mathbf{u}$ are

$$\mathbf{u} = \mathbf{R} - \mathbf{R}_0 = (u_x, u_y, z)\,, \tag{1}$$

where (u_x, u_y, z) are the Cartesian coordinates of $\mathbf{u}$, and the coordinate $z(\mathbf{r}) \equiv z(x, y)$ represents the out-of-plane displacement. The spatial derivatives of the displacement coordinates are

$$\partial_j u_i = \frac{\partial u_i}{\partial j}, \quad \partial_i z = \frac{\partial z}{\partial i}, \ (i, j = x, y). \tag{2}$$

These derivatives define the components of the local in-plane strain tensor of the membrane [18]

$$\epsilon_{ij} = \frac{1}{2}(\partial_i u_j + \partial_j u_i) + \frac{\partial_i z \partial_j z}{2} + \epsilon \delta_{ij}. \tag{3}$$

Here, the linear strain ϵ defines a preexisting uniform biaxial strain and δ_{ij} is the Kronecker delta.

The flat crystalline membrane can be considered as made of $N_a \times N_a$ square cells with cell parameter a. The in-plane area S_p is a square of length L,

$$S_p = L^2 = L_0^2(1+\epsilon)^2 = (N_a a)^2\,, \tag{4}$$

where L_0 is the side length of the unstrained membrane ($\epsilon = 0$). The Brillouin zone (BZ) in reciprocal space is defined, for uneven N_a, by the set of discrete points

$$\{\mathbf{q}\} = \left\{\frac{2\pi}{L}(l_x, l_y)\right\}^{\diamond}, \quad \text{with } l_x, l_y = -\frac{N_a - 1}{2}, \ldots, 0, \ldots, \frac{N_a - 1}{2}. \tag{5}$$

The diamond $\diamond$ means that the origin of the BZ with $l_x = l_y = 0$ is omitted from the set of points. The $\mathbf{q}$ points with the lowest modulus, $q = 2\pi/L$, are labeled as q_{10} and q_{01}, respectively, where the subscript shows the values of the coordinates (l_x, l_y). The spectrum of out-of-plane fluctuations is defined by the Fourier transform of $z(\mathbf{r})$ as

$$A_{\mathbf{q}} = \frac{1}{L^2} \int_0^L \int_0^L dxdy\, z(\mathbf{r})\, e^{-i\mathbf{q}\mathbf{r}}\,, \tag{6}$$

where $\mathbf{q} = (q_x, q_y)$ is a vector of the discretized BZ.

B. Elastic energy

The local elastic energy of a solid membrane is defined as

$$e_t = e_b + e_s \,, \tag{7}$$

where e_b and e_s are the elastic energy density for the bending and strain deformations, respectively [18,19],

$$e_b = \frac{1}{2}\kappa_0\big(\partial^2_{xx}z + \partial^2_{yy}z\big)^2 = \frac{1}{2}\kappa_0(\nabla^2 z)^2 \,, \tag{8}$$

$$e_s = \mu_0\big(\epsilon^2_{xx} + \epsilon^2_{yy} + 2\epsilon^2_{xy}\big) + \frac{\lambda_0}{2}(\epsilon_{xx} + \epsilon_{yy})^2. \tag{9}$$

∇^2 is the Laplacian, κ_0 is the bending modulus, and μ_0 and λ_0 are the in-plane Lame coefficients.

The total elastic energy is

$$E_t = \int_0^L\int_0^L dxdy\; e_t(x, y) \,, \tag{10}$$

with similar expressions for the total bending and strain energies, E_b and E_s, respectively.

By working in Fourier space, and integrating the Gaussian degrees of freedom associated to the in-plane displacement coordinates (u_x, u_y), one gets that the configurational partition function of a solid membrane can be written as a function of a new effective elastic energy E as [6]

$$Z_{N\epsilon T} = \prod_{\mathbf{q}}^{BZ}\int dA_{\mathbf{q}}\; \alpha(q)\exp\left(-\beta E\right) , \tag{11}$$

where $\beta = 1/k_BT$ is proportional to the inverse temperature T, and k_B is the Boltzmann constant. $\alpha(q)$ is

$$\alpha(q) = 2(1-\nu_0)(1+\nu_0)^2\left(\frac{\pi}{\beta Y_0 L^2 q^2}\right)^2. \tag{12}$$

ν_0 is the Poisson ratio, and Y_0 is the Young modulus. The square modulus of $\mathbf{q}$ is $q^2 = q_x^2 + q_y^2$. The effective elastic energy E defines the Nelson-Peliti Hamiltonian. It is composed of the following summands:

$$E = E_p + E_r + E_b + E_i. \tag{13}$$

E_p and E_r are energy terms that depend explicitly on the uniform strain ϵ. E_p is the elastic energy due to the strain of the projected area L^2,

$$E_p = 2B_0L^2\epsilon^2 \,, \tag{14}$$

where $B_0 = \mu_0 + \lambda_0$ is the 2D compressibility modulus of the nondeformed layer. E_r is the elastic energy related to the coupling between the strain ϵ and the excess area of the membrane [see Eq. (20) below],

$$E_r = 2B_0L^2\epsilon\sum_{\mathbf{q}}^{BZ}\frac{q^2|A_{\mathbf{q}}|^2}{2}. \tag{15}$$

E_b is the total bending energy, that in Fourier space becomes

$$E_b = \sum_{\mathbf{q}}^{BZ}\frac{1}{2}L^2\kappa_0 q^4|A_{\mathbf{q}}|^2. \tag{16}$$

E_i is the effective interaction energy between the in-plane and out-of-plane membrane modes [6]

$$E_i = \sum_{\mathbf{q}}^{BZ}\frac{1}{8}L^2Y_0|\Psi(\mathbf{q})|^2 \,, \tag{17}$$

where

$$\Psi(\mathbf{q}) = \frac{1}{q^2}\big[q_y^2C_{xx}(\mathbf{q}) + q_x^2C_{yy}(\mathbf{q}) - 2q_xq_yC_{xy}(\mathbf{q})\big] \,, \tag{18}$$

and

$$C_{ij}(\mathbf{q}) = \sum_{\mathbf{k}}^{BZ} -k_i(q_j - k_j)A_{\mathbf{k}}A_{\mathbf{q}-\mathbf{k}}. \tag{19}$$

E_r and E_b are harmonic (quadratic) energy terms proportional to $|A_{\mathbf{q}}|^2$. The interaction energy E_i is anharmonic with quartic dependence on $A_{\mathbf{q}}$. It is calculated via products of amplitudes of four out-of-plane modes $A_{\mathbf{k}}A_{\mathbf{q}-\mathbf{k}}A_{\mathbf{k}'}A_{\mathbf{q}'-\mathbf{k}'}$. The relationship between the interaction energy E_i, and the Gaussian curvature of the membrane is presented in Appendix A.

The true real area S_r of the membrane is larger than the projected one, $S_p = L^2$, as a consequence of the finite amplitude of the out-of-plane fluctuations $A_{\mathbf{q}}$. Both areas are related as [20,21]

$$S_r = S_p\left(1 + \sum_{\mathbf{q}}^{BZ}\frac{q^2|A_{\mathbf{q}}|^2}{2}\right). \tag{20}$$

The difference between the real and projected areas, $S_r - S_p$, has been referred earlier as the excess area or hidden area of the membrane [21,22]. The excess area of graphene has been studied experimentally by Raman spectroscopy [23].

C. Stress

The Helmholtz free energy of the membrane is defined as

$$F = -k_BT\ln Z_{N\epsilon T}. \tag{21}$$

The stress τ is the intensive variable conjugate to the projected area,

$$\tau = -\left(\frac{\partial F}{\partial S_p}\right)_{N,T} = -\left\langle\frac{\partial E}{\partial S_p}\right\rangle = -\frac{1}{2LL_0}\left\langle\frac{\partial E}{\partial \epsilon}\right\rangle. \tag{22}$$

The angular brackets indicate an ensemble average over the collective defined by the partition function $Z_{N\epsilon T}$. In the calculation of $\partial E/\partial\epsilon$ we have considered the explicit dependence of E on ϵ, as well as the implicit dependence through L and $\mathbf{q}$, as $L = L_0(1+\epsilon)$, and $\mathbf{q} \propto 2\pi/L$. There appear four contributions to the membrane stress

$$\tau = \tau_p + \tau_r + \tau_b + \tau_i \,, \tag{23}$$

where

$$\tau_p = -B_0(2\epsilon + 4\epsilon^2), \tag{24}$$

$$\tau_r = -B_0(1+\epsilon)\sum_{\mathbf{q}}^{BZ}\frac{q^2\langle|A_{\mathbf{q}}|^2\rangle}{2}, \tag{25}$$

$$\tau_b + \tau_i = \frac{\langle E_b\rangle + \langle E_i\rangle}{L^2}. \tag{26}$$

TABLE I. Elastic constants employed in the Nelson-Peliti Hamiltonian. κ_0 is the bending modulus, μ_0 and λ_0 are the Lamé coefficients, B_0 is the 2D compressional modulus (analogous to the bulk modulus in 3D), Y_0 is the uniaxial Young modulus, and ν_0 is the Poisson ratio. Numerical values correspond to the empirical LCBOPII potential model for carbon-carbon interactions in graphene [27,36].

κ_0	1.49 eV	
μ_0	9.29 eV/Å^2	
λ_0	3.36 eV/Å^2	
B_0	12.65 eV/Å^2	$\mu_0 + \lambda_0$
Y_0	21.43 eV/Å^2	$\frac{4\mu_0(\mu_0+\lambda_0)}{2\mu_0+\lambda_0}$
ν_0	0.153	$\frac{\lambda_0}{2\mu_0+\lambda_0}$

The quantity 2ϵ in the expression of τ_p is to first order in ϵ the strain of the projected area of the membrane S_p [see Eq. (4)]. The sum over $\mathbf{q}$ vectors in τ_r represents an additional surface strain caused by the surface ripples [see Eq. (20)].

III. MC SIMULATIONS

The elastic constants in the Nelson-Peliti Hamiltonian ($\kappa_0, \mu_0, \lambda_0$) have been chosen as those corresponding to graphene and are summarized in Table I. The unstrained membrane is defined by a square supercell with periodic boundary conditions and area $L_0^2 = (N_a a_0)^2$, where the distance $a_0 = 2.46$ Å is taken equal to the lattice parameter of graphene. This choice implies that the largest modulus of the $\mathbf{q}$ vectors in the BZ is $q = \pi/a_0$ (ultraviolet cut-off). The surface density of graphene is attained by considering that the supercell contains N carbon atoms

$$N = \frac{L_0^2}{s_0} = \frac{(N_a a_0)^2}{s_0} = \frac{4}{\sqrt{3}} N_a^2 , \tag{27}$$

where s_0 is the specific surface area of graphene, $s_0 = \sqrt{3}a_0^2/4 = 2.619$ Å^2/atom.

Periodic boundary conditions are commonly used in computer simulations to mitigate the influence of membrane's boundaries and finite-size effects. In the presence of a tensile strain, $\epsilon > 0$, the (x, y) plane on which the periodic conditions are applied is physically well determined. This is the plane on which the strain of the projected area of the membrane, or its conjugated stress, are externally controlled as thermodynamic variables. It is worth noting that the most likely experimental scenario would involve rigidly clamping the edges of the membrane to pieces of the substrate, so that the out-of-plane and the in-plane displacements are constrained to vanish at the boundary. This scenario differs from the periodic conditions used in our simulations. As the effective interaction E_i between the collective variables of the Nelson-Peliti Hamiltonian is long ranged, one may worry that different choices of boundary conditions could lead to inequivalent thermodynamic behavior. However, we will demonstrate in Sec. IV B that as the tensile strain ϵ increases, the contribution of the (long-ranged) interaction energy $\langle E_{i,q}\rangle$ to the elastic energy is significantly reduced for the long-wavelength limit of small q.

In the limit where $\epsilon = 0$, the use of periodic boundary conditions should be regarded with further caution, since the boundary conditions are applied on a (x, y) plane that has no physical significance. In the case of a freely floating membrane, the projected area on any plane would exhibit huge fluctuations, which are strongly (and rather artificially) constrained on the specific plane chosen for imposing periodic boundary conditions. Nevertheless, our simulation results for $\epsilon = 0$ align well with the small $\epsilon > 0$ limit [see Fig. 5(c) below]. Thus, we can reasonably conclude that, as is commonly assumed in most simulation studies of free standing membranes, periodic boundary conditions are a suitable choice for investigating size-independent properties that effectively represent large experimental systems.

Averaged quantities as a function of temperature and system size were derived from the configurational partition function in Eq. (11) using classical MC simulations. As the elastic energy E is formulated in $\mathbf{q}$ space, the complex amplitudes $A_\mathbf{q}$ are sampled as random variables in the MC simulations. Inversion symmetry in $\mathbf{q}$ space, $A_{-\mathbf{q}} = A_\mathbf{q}^*$, allows us to consider $\mathbf{q}$ vectors in one-half of the BZ as independent variables, with the consequent reduction of computer time in the simulations.

As our main interest lies in the study of long-wavelength oscillations with small $\mathbf{q}$ values, an ultraviolet cut-off radius, q_c, has been considered in the BZ, so that $A_\mathbf{q} \equiv 0$, whenever $q > q_c$. The actual number of $\mathbf{q}$ points, with modulus lower than q_c, included in the MC simulation will be denoted as $N_\mathbf{q}$. We have used $q_c = 0.3$ Å^{-1} in our simulations. This cut-off does not significantly affect the average amplitudes $\langle A_\mathbf{q}\rangle$ when $q < 0.08$ Å^{-1}. The main effect of using a cut-off $q_c = 0.3$ Å^{-1}, instead of the value at the boundary of the BZ, $q_c = \pi/a_0 = 1.3$ Å^{-1}, is that the average stress of the layer is shifted by a constant positive value. This shift is due to the truncated summation of $q^2|A_\mathbf{q}|^2$ in Eq. (25). The sum increases monotonically as the cut-off q_c increases. At 300 K the shift in the stress τ amounts to 0.02 eV/Å^2 when $q_c = 0.3$ Å^{-1}. This value is nearly independent of the strain of the layer and the size of the membrane (when $N > 10^5$ atoms) and increases linearly with the temperature. The main conclusions of our study are unaffected by this shift. Therefore, all simulation results in Sec. IV were obtained using a cut-off value of $q_c = 0.3$ Å^{-1}, except for an analysis in Sec. IV I regarding the impact of this cut-off on the stability of the flat morphology of the membrane.

In the calculation of the correlation functions $C_{ij}(\mathbf{q})$ in Eq. (19), the translational symmetry in $\mathbf{q}$ space has been considered. Whenever a vector $\mathbf{q} - \mathbf{k}$ lies outside the first BZ, a reciprocal translation vector $\mathbf{Q}$ has been selected, so that the translated vector

$$\mathbf{t} = \mathbf{q} - \mathbf{k} + \mathbf{Q} \tag{28}$$

lies within the first BZ. The amplitude $A_\mathbf{t}$ and the coordinates of the translated vector $\mathbf{t}$ were used in the calculation of $C_{ij}(\mathbf{q})$.

The MC sampling of the complex amplitude $A_\mathbf{q}$ is performed by setting an acceptance criterion of ∼50% in the MC trials. The maximum random move for each $A_\mathbf{q}$ depends strongly on the q value. Long-wavelength fluctuations with small q display large amplitudes, and accordingly require larger random moves than fluctuations with higher values of

q. This fact is relevant to the efficiency of the MC sampling [13,14].

MC simulations have been performed in a temperature range between 1 and 2000 K. System sizes were studied between 10^4 to 2.2×10^6 atoms, which correspond to lateral sizes between $L = 298$ Å and $L = 2380$ Å. The lowest q modulus in the simulation is $2\pi/L$ (infrared cut-off), which takes a value between 2.1×10^{-2}Å^{-1} and 2.6×10^{-3} Å^{-1} depending on the membrane size.

A MC step (MCS) implies an attempt to randomly modify each of the amplitudes $A_{\mathbf{q}}$. Typical MC runs imply 2×10^4 MCS for equilibration followed by 10^5 MCS for thermal averages. Calculated equilibrium properties are the spectrum of flexural mode amplitudes $\langle|A_{\mathbf{q}}|^2\rangle$, as well as the energy partitioning into bending $\langle E_b\rangle$, interaction $\langle E_i\rangle$, and strain-dependent contributions $\langle E_p\rangle$ and $\langle E_r\rangle$.

Some MC simulations have been performed in the $N\tau T$ ensemble, to check their consistency with the $N\epsilon T$ simulations. The relevant thermodynamic potential in the $N\tau T$ ensemble is the enthalpy, $H = E + \tau S_p$, and the random variables to be sampled are the out-of-plane amplitudes $A_{\mathbf{q}}$, and the uniform strain ϵ. The acceptance rate for the sampling of ϵ was set at ~90%.

IV. RESULTS

The most studied property of a crystalline membrane with the Nelson-Peliti Hamiltonian is the long-wavelength limit of the out-of-plane fluctuations. However, it is also of interest to study the temperature dependence of the elastic energy, its partition into bending and interaction contributions, as well as its partition into q dependent contributions. The presentation of our results starts with this energy analysis.

A. Average elastic energy

The number of degrees of freedom in our simulations is equal to the number of $\mathbf{q}$ points, $N_{\mathbf{q}}$. The classical equipartition and virial theorems imply that the average kinetic and potential energies of the membrane are not independent quantities. The equipartition theorem dictates that the average kinetic energy of each degree of freedom is $k_BT/2$, while the virial theorem establishes that quadratic terms (E_r, E_b) have average potential energies equal to their kinetic energy contribution, while quartic terms (E_i) display average potential energies that are one-half of their kinetic energy [24,25], namely

$$N_{\mathbf{q}}\frac{k_BT}{2} = \langle E_r\rangle + \langle E_b\rangle + 2\,\langle E_i\rangle. \tag{29}$$

We consider first the case of an unstrained membrane $(\epsilon = 0)$, where the energy terms $E_p = E_r = 0$. The average bending $\langle E_b\rangle$, and interaction energies $\langle E_i\rangle$ are displayed as a function of temperature in Fig. 1(a). The average elastic energy is $\langle E\rangle = \langle E_b\rangle + \langle E_i\rangle$. These results correspond to a membrane with lateral dimension $L = 1188$Å. The cut-off radius in the BZ was $q_c = 0.3$ Å^{-1}, so that $N_{\mathbf{q}} = 5048$ vectors were included in the MC simulation. For this system size ($N = 5.4\times10^5$ atoms), the smallest q modulus is $2\pi/L = 5\times10^{-3}$ Å^{-1}. The elastic energy $\langle E\rangle$ is lower than $k_BT/2$ at any finite temperature, while the harmonic bending energy $\langle E_b\rangle$ is larger than the anharmonic $\langle E_i\rangle$ contribution.

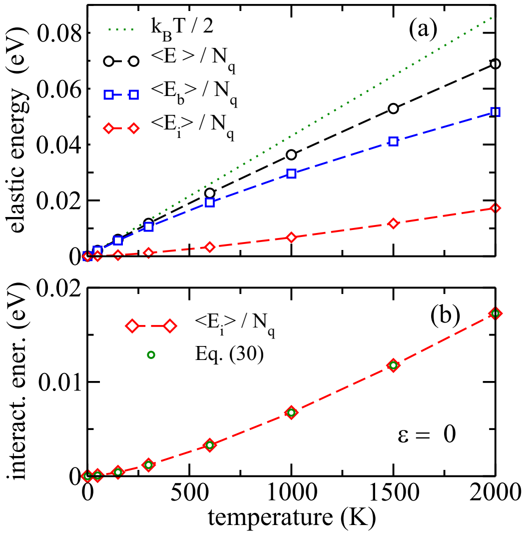

FIG. 1. (a) Thermal average of the elastic, $\langle E\rangle$, bending, $\langle E_b\rangle$, and interaction, $\langle E_i\rangle$, energy as a function of temperature for an unstrained membrane $(\epsilon = 0)$ with size $L_0 = 1188$ Å ($N = 5.4\times10^5$ atoms). The elastic energy is $\langle E\rangle = \langle E_b\rangle + \langle E_i\rangle$. All energies are normalized by the number of modes $N_{\mathbf{q}}$. At any finite temperature $\langle E\rangle/N_{\mathbf{q}}$ is lower than $k_BT/2$. (b) The average interaction energy $\langle E_i\rangle$ is compared to the result from the equipartition and virial theorems in Eq. (30). Dashed lines are guides to the eye. The cut-off radius in the simulation was $q_c = 0.3$ Å^{-1}.

The equipartition and virial theorems predict that the average bending and interaction energies of the membrane are not independent. After Eq. (29), if $E_r = 0$,

$$\langle E_i\rangle = N_{\mathbf{q}}\frac{k_BT}{4} - \frac{\langle E_b\rangle}{2}. \tag{30}$$

The data displayed Fig. 1(b) show that the temperature dependence of $\langle E_i\rangle$ derived from the simulations agrees with this prediction.

B. Mode-dependent elastic energy

We now consider the mode-dependent elastic energy of a membrane with finite strain $(\epsilon \geqslant 0)$. If $\epsilon > 0$ then the elastic energy related to the excess area is finite, $E_r > 0$. E_r, as well as the elastic bending energy E_b are expressed as a sum over independent $\mathbf{q}$ modes [see Eqs. (15) and (16)]. These $\mathbf{q}$ mode contributions are

$$E_{r,\mathbf{q}} = 2B_0L^2\epsilon\frac{q^2|A_{\mathbf{q}}|^2}{2}. \tag{31}$$

$$E_{b,\mathbf{q}} = \frac{1}{2}L^2\kappa_0q^4|A_{\mathbf{q}}|^2\,, \tag{32}$$

The interaction energy E_i in Eq. (17) can not be separated into independent $\mathbf{q}$ contributions. Nevertheless, the virial theorem can be applied to define the average value of this energy term,

$$\langle E_{i,\mathbf{q}}\rangle = \frac{k_BT}{4} - \frac{\langle E_{b,\mathbf{q}}\rangle + \langle E_{r,\mathbf{q}}\rangle}{2}. \tag{33}$$

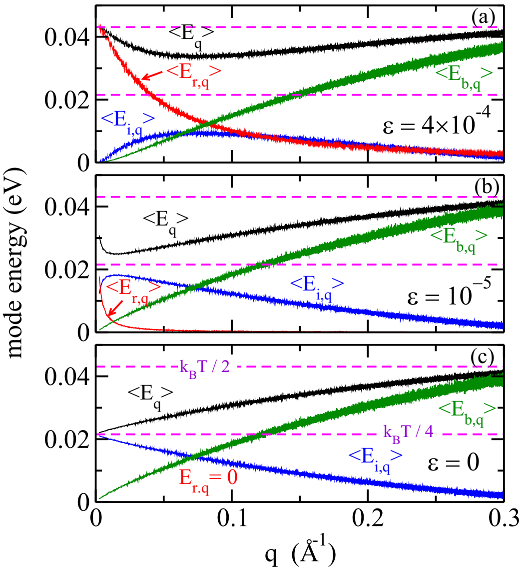

FIG. 2. Partition of the elastic energy into q-dependent terms: bending $\langle E_{b,q}\rangle$, interaction $\langle E_{i,q}\rangle$, excess area contribution $\langle E_{r,q}\rangle$, as well as their sum $\langle E_q\rangle = \langle E_{b,q}\rangle + \langle E_{i,q}\rangle + \langle E_{r,q}\rangle$. The results are shown at 1000 K for a membrane with $N = 2.2\times10^6$ atoms. For this system size, the smallest q modulus is $2\pi/L = 2.6\times10^{-3}$ Å^{-1}. The cut-off radius in the simulation was $q_c = 0.3$ Å^{-1}. The results are shown for three different biaxial strains: (a) $\epsilon = 4\times10^{-4}$; (b) $\epsilon = 10^{-5}$; (c) $\epsilon = 0$. The dashed horizontal lines mark the energies $k_BT/2$ and $k_BT/4$, respectively.

The partition of the elastic energy of each mode is then

$$\langle E_{\mathbf{q}}\rangle = \langle E_{r,\mathbf{q}}\rangle + \langle E_{b,\mathbf{q}}\rangle + \langle E_{i,\mathbf{q}}\rangle. \tag{34}$$

The average elastic energy of the vibrational modes for a membrane with $L_0 = 2378$ Å ($N = 2.2\times10^6$ atoms) is displayed in Fig. 2 at a temperature of 1000 K for three different strains: (a) $\epsilon = 4\times10^{-4}$, (b) $\epsilon = 10^{-5}$, and (c) $\epsilon = 0$. The cut-off radius in reciprocal space was $q_c = 0.3$ Å^{-1}, i.e., $N_{\mathbf{q}} = 20250$ vectors were explicitly treated in the simulations.

Let us consider first the simplest case where $\epsilon = 0$, and then $E_{r,\mathbf{q}} = 0$, [see Fig. 2(c)]. The anharmonic interaction energy $\langle E_{i,\mathbf{q}}\rangle$ dominates over the bending energy $\langle E_{b,\mathbf{q}}\rangle$ for $q < 0.07$ Å^{-1}. As q increases, the bending energy tends to $k_BT/2$, while the interaction energy tends to vanish. However, in the long-wavelength limit of small q, the average interaction energy $\langle E_{i,\mathbf{q}}\rangle$ approaches the limit $k_BT/4$, while the harmonic bending energy $\langle E_{b,\mathbf{q}}\rangle$ tends to vanish.

The presence of biaxial strain modifies completely the long-wavelength behavior. When $\epsilon = 4\times10^{-4}$, Fig. 2(a) shows that the harmonic elastic energy associated with the excess area $\langle E_{r,\mathbf{q}}\rangle$ becomes the dominant energy in the limit $q \to 0$. This result is in line with the SCSA predictions and the MC results of Ref. [17]. As a consequence of the harmonic character of $E_{r,\mathbf{q}}$, this average energy tends to $k_BT/2$ at small q.

The results in Fig. 2(b) for $\epsilon = 10^{-5}$ show that the smaller the strain ϵ the smaller the value of q where the excess area term $\langle E_{r,\mathbf{q}}\rangle$ dominates over the anharmonic interaction $\langle E_{i,\mathbf{q}}\rangle$.

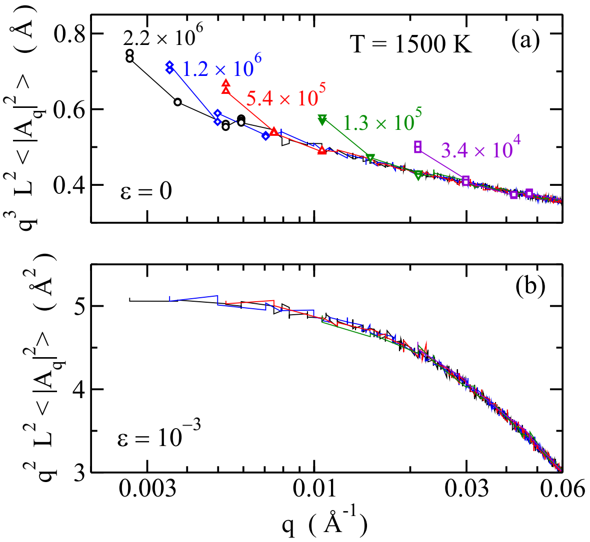

FIG. 3. (a) The function $q^3L^2\langle|A_{\mathbf{q}}|^2\rangle$ is displayed as a function of q for different system sizes. The data correspond to MC simulations of an unstrained membrane ($\epsilon = 0$) at $T = 1500$ K. The number of atoms N in the simulations is indicated. (b) The functions $q^2L^2\langle|A_{\mathbf{q}}|^2\rangle$ are shown for membranes with the same sizes and temperature as in panel (a), but for a finite strain $\epsilon = 10^{-3}$. Results at discrete q values are connected by straight lines. The x axis is displayed with a logarithmic scale. The cut-off for the simulations was $q_c = 0.3$ Å^{-1}.

C. Amplitude of out-of-plane fluctuations

In this subsection we focus on the average of the square amplitude of the out-of-plane fluctuations $\langle|A_{\mathbf{q}}|^2\rangle$. This average is expected to vary with the size of the membrane as L^{-2}. The reason is that the mode-dependent bending energy depends on the factor $L^2\langle|A_{\mathbf{q}}|^2\rangle$ [see Eq. (32)], and the bending energy $\langle E_{b,\mathbf{q}}\rangle$ remains nearly constant as the size of the membrane varies.

The average amplitudes $\langle|A_{\mathbf{q}}|^2\rangle$ are displayed as a function of q for a membrane with vanishing strain ($\epsilon = 0$) in Fig. 3(a). We have represented the function $q^3L^2\langle|A_{\mathbf{q}}|^2\rangle$ for membranes with different lateral dimensions in the interval $L = 298$ to 2378 Å, containing between 3.4×10^4 and 2.2×10^6 atoms.

We observe a conspicuous finite-size effect only for the two q points with lowest modulus ($2\pi/L$) for each membrane size (i.e., q_{10} and q_{01}). This finite-size effect was reported by Tröster in his MC simulations of an unstrained membrane [13,14]. He attributed this effect to the anisotropic character of the correlation in Eq. (19), which is required for the calculation of the interaction energy E_i. Correlation between out-of-plane amplitudes causes a decrease in their modulus. Thus, if the interaction term E_i were suppressed from the Hamiltonian, the out-of-plane amplitudes would increase significantly. The anisotropy is related to the fact that the origin of the BZ is excluded from the set of $\mathbf{q}$ points where the correlation function is calculated. In the BZ, The points q_{10} and q_{01} have the special geometric property that they are the only ones that do not have neighboring $\mathbf{q}$ points between them and the origin. This causes the modulus of the amplitudes corresponding to q_{10} and q_{01} to display anomalously large values. Finite-size effects at $\mathbf{q}$ vectors with modulus larger than $2\pi/L$ are inappreciable in the scale of Fig. 3(a). The size effect at q_{10} and q_{01} will be quantified as a function of the temperature and membrane size in Sec. IV E.

Average amplitudes for the case of finite biaxial strain, $\epsilon = 10^{-3}$, are displayed in Fig. 3(b) for membranes with the same number of atoms as in panel (a). The finite tensile biaxial strain ($\epsilon > 0$) affects drastically the q dependence of the average amplitudes $\langle |A_{\mathbf{q}}|^2 \rangle$, in comparison to the case $\epsilon = 0$. The amplitudes in Fig. 3(b) are displayed as $q^2 L^2 \langle |A_{\mathbf{q}}|^2 \rangle$. This function tends to a constant value in the limit $q \to 0$. The finite-size effect observable at q_{10} and q_{01} when $\epsilon = 0$ is absent in the case of finite strain. The q dependence of the average amplitudes $\langle |A_{\mathbf{q}}|^2 \rangle$ as a function of the strain ϵ is analyzed in the next subsection.

D. Numerical fit of the out-of-plane amplitudes

The amplitudes of the out-of-plane fluctuations will be analyzed with the function

$$f_q = \frac{1}{\beta L^2 \langle |A_{\mathbf{q}}|^2 \rangle}. \quad (35)$$

f_q will be then fitted by an appropriate numerical model. In the context of biological membranes the function f_q/q^2 has been associated with a q-dependent surface tension [20], while in the context of solid membranes f_q has been considered as an approximation to the dispersion relation of the out-of-plane modes $\rho\omega_q^2$, where ρ is the surface density and ω_q is the wavenumber of the mode [17,26,27].

The MC results for $\langle |A_{\mathbf{q}}|^2 \rangle$ in the presence of finite biaxial strain are analyzed first. Both the SCSA and variational perturbation theory predict that in this case the long-wavelength dependence of f_q is

$$f_q = \sigma q^2, \quad (36)$$

where $\sigma = 2B_0\epsilon$, to first order in ϵ [6,17]. Our MC simulations of f_q have been fitted by a least-squares method to the function σq^2. The least-squares fits are performed with weighting factors $w_q \propto f_q^{-2}$. In this way, the region of small q is given a larger weight. The fitted value of σ in the interval $[2\pi/L, q_{\text{end}}]$ is presented in Fig. 4 as a function of q_{end}. The result corresponds to a simulation at a temperature of 1000 K, lateral dimension $L = 2380$ Å, and strain $\epsilon = 10^{-3}$. The extrapolated value of σ in the long-wavelength limit ($q_{\text{end}} \to 0$) is

$$\sigma = -\tau_p = B_0(2\epsilon + 4\epsilon^2). \quad (37)$$

This result is in agreement with previous studies with the Nelson-Peliti Hamiltonian [6,17].

When the strain vanishes, $\epsilon = 0$, the expectation of the SCSA and RG approximation is that the amplitudes of the out-of-plane fluctuations in the long-wavelength limit are determined by a critical exponent η [7–9,12], i.e.,

$$f_q = \gamma q^{4-\eta}. \quad (38)$$

We have considered the following trial function to fit our simulation results of f_q,

$$f_q = \sigma q^2 + \gamma q^{4-\eta}. \quad (39)$$

σ, γ, and the exponent $4-\eta$ are the fitting parameters. This function has the flexibility to describe the expected long-wavelength limit in the case of an unstrained membrane ($\epsilon = 0$). as well as in the presence of a finite biaxial strain ($\epsilon > 0$).

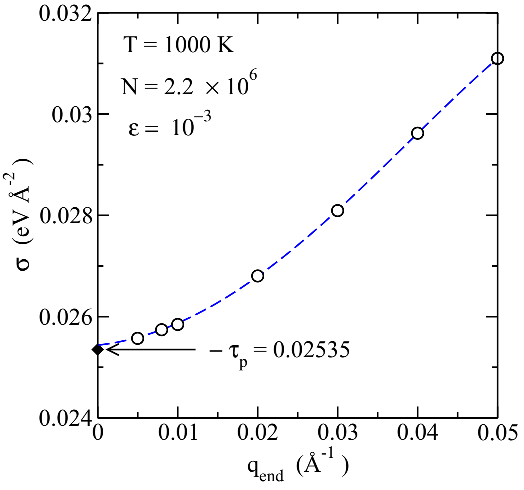

FIG. 4. Result of the least-squares fit of the simulation results of $f_q = 1/\beta L^2 \langle |A_{\mathbf{q}}|^2 \rangle$ to the function σq^2 in the interval $[2\pi/L, q_{\text{end}}]$. The value of σ is represented as a function of q_{end}. The dashed line is a cubic fit. The simulation was performed at 1000 K for a membrane with lateral dimension $L = 2380$ Å ($N = 2.2\times 10^6$ atoms) and strain $\epsilon = 10^{-3}$. In the long-wavelength limit ($q_{\text{end}} \to 0$), the fitted value converges to $\sigma = -\tau_p = B_0(2\epsilon + 4\epsilon^2)$.

The fitted values (σ, γ, and $4-\eta$) obtained by the least-squares analysis of our MC results are displayed in Fig. 5 as a function of the strain ϵ. The data were obtained at 1000 K

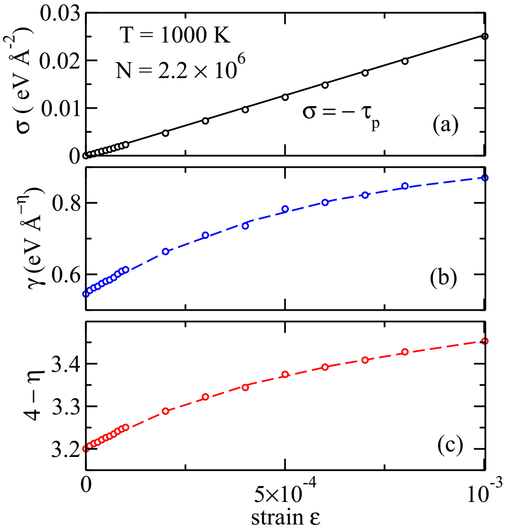

FIG. 5. Results of the least-squares fitting of the simulation data of f_q to the function $\sigma q^2 + \gamma q^{4-\eta}$. The fitted parameters σ, γ, and $4-\eta$ are displayed as a function of the strain ϵ in the panels (a), (b), and (c), respectively. In panel (a), the continuous line represents the stress term $-\tau_p = B_0(2\epsilon + 4\epsilon^2)$. The value of the critical exponent when the strain $\epsilon = 0$ is $\eta = 0.8$ [see panel (c)]. The simulations were performed at 1000 K for a crystalline membrane with lateral size $L \simeq 2380$ Å ($N = 2.2\times 10^6$) and a cut-off $q_c = 0.3$ Å^{-1}. Dashed lines are guides to the eye.

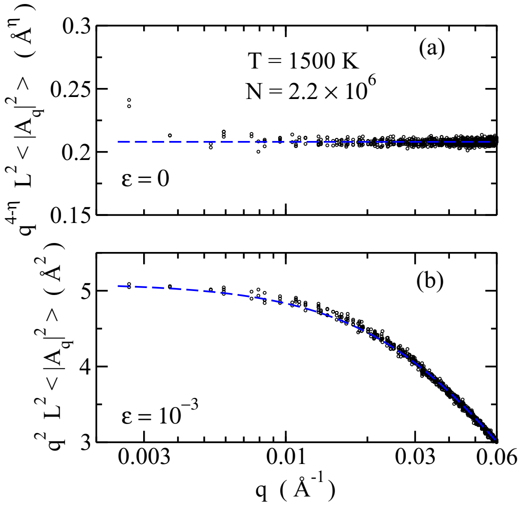

FIG. 6. Comparison of the functions of the square amplitudes $\langle|A_{\mathbf{q}}|^2\rangle$ displayed in Fig. 3 for a membrane with size $N = 2.2\times10^6$ atoms, with the results derived from the least-squares fit of the function f_q in Eq. (35). Discrete points are simulation results at a temperature of 1500 K, while the dashed line is the least-squares fit. The employed cut-off is $q_c = 0.3$ Å^{-1}. The results are shown for (a) strain $\epsilon = 0$. Here the square amplitudes $\langle|A_{\mathbf{q}}|^2\rangle$ are presented as the function $q^{4-\eta}L^2\langle|A_{\mathbf{q}}|^2\rangle$, with the critical exponent $\eta = 0.8$; (b) strain $\epsilon = 10^{-3}$.

for a membrane with lateral dimension $L \simeq 2380$Å (the actual length L is a function of the strain ϵ). The q interval used in the fit was $[2\pi/L, 0.08$ Å$^{-1}]$. When $\epsilon = 0$, the two points q_{10} and q_{01}, with modulus $2\pi/L$, were omitted from the fitting interval, as their amplitudes $\langle|A_{\mathbf{q}}|^2\rangle$ display noticeable finite-size effects.

The fitted values of the tension σ follow the relation in Eq. (37). Thus, for finite strain, $\epsilon > 0$, the long-wavelength behavior of f_q is determined by the term $-\tau_p q^2$. When the strain $\epsilon = 0$, σ and τ_p vanish, and the long-wavelength behavior of f_q is determined by $\gamma q^{4-\eta}$, where η is the critical exponent. Six different MC simulations were performed at temperatures between 500 and 2000 K to derive an average value of $\eta = 0.80 \pm 0.01$. This number is in good agreement with the one reported by Tröster in his MC simulations [13,14]. The parameter γ increases monotonically with the biaxial strain at a given fixed temperature.

The simulated square amplitudes $\langle|A_{\mathbf{q}}|^2\rangle$ plotted in Fig. 3 for $N = 2.2\times10^6$ atoms at 1500 K are compared with the results obtained by the least-squares fit of the function f_q in Fig. 6. The fitted function reproduces reasonably well the average amplitudes obtained in the simulations for the strains $\epsilon = 0$ and 10^{-3}, respectively. The most visible deviation between simulation and fitted data is the finite-size effect of the points q_{10} and q_{01} when the strain is $\epsilon = 0$. The magnitude of this effect is studied in the next subsection as a function of the size of the membrane and the temperature.

E. Finite-size effect in the out-of-plane amplitudes at q_{10} and q_{01}

The finite-size effect in the out-of-plane amplitudes $\langle|A_{\mathbf{q}}|^2\rangle$ at the points q_{10} and q_{01} of the unstrained layer $(\epsilon = 0)$ is quantified by calculating first the expected value of the amplitude $A^2_{\mathbf{q},\mathrm{fit}}$ using the fitted model for f_q,

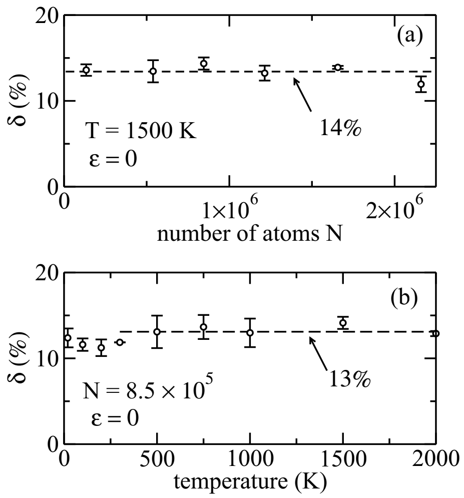

FIG. 7. Magnitude of the finite-size error δ defined at the reciprocal points q_{10} and q_{01} for an unstrained membrane $(\epsilon = 0)$. (a) δ as a function of the size of the membrane at a temperature of 1500 K. (b) δ as a function of the temperature for a membrane with 8.5×10^5 atoms.

$$A^2_{\mathbf{q},\mathrm{fit}} = \frac{1}{\beta L^2 \gamma q^{4-\eta}} , \tag{40}$$

and then calculating the relative deviation $\delta_{\mathbf{q}}$,

$$\delta_{\mathbf{q}} = \frac{\langle|A_{\mathbf{q}}|^2\rangle - A^2_{\mathbf{q},\mathrm{fit}}}{\langle|A_{\mathbf{q}}|^2\rangle}. \tag{41}$$

The finite-size effect is quantified as the average of $\delta_{\mathbf{q}}$ for the points q_{10} and q_{01},

$$\delta = 100 \times \left(\frac{\delta_{10} + \delta_{01}}{2}\right). \tag{42}$$

We have studied the dependence of δ with the number of atoms and the temperature in Fig. 7. In panel (a) the magnitude of δ at 1500 K is displayed for membrane with sizes between 1.3×10^5 and 2.2×10^6 atoms. We find that the finite-size effect is rather independent of the size of the membrane, and the value of δ is about 14%. This result is in reasonable agreement with the value of $\delta \sim 12\%$ given in Refs. [13,14]. In simulations with temperatures between 20 and 2000 K for a fixed size of 8.4×10^5 one gets that $\delta \sim 13\%$ [see Fig. 7(b)]. The independence of the value of δ with the membrane size and the temperature, as well as the appearance of this size effect only when $\epsilon = 0$, is in line with the consideration that this effect is related to the anisotropy of the convolution in Eq. (19).

F. Stress-strain curves

The isothermal stress-strain curve $\tau - \epsilon$ of a crystalline membrane is displayed in Fig. 8(a) at 1000 K. The data were derived by $N\epsilon T$ simulations with a cut-off $q_c = 0.3$Å^{-1} for several sizes between 1.3×10^5 and 2.2×10^6 atoms. For strains $\epsilon \geqslant 0$ the stress at 1000 K is always tensile, i.e.,

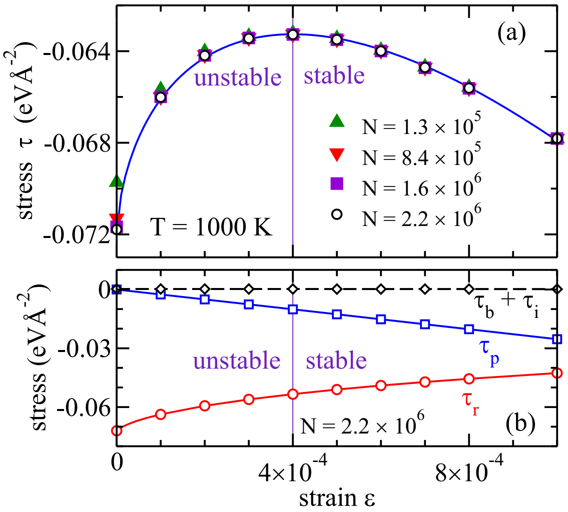

FIG. 8. (a) Isothermal stress-strain curve at 1000 K as derived from MC simulations for membranes with different sizes in the $N\epsilon T$ ensemble. The maximum of the curve is a critical point. (b) The four contributions to the stress, $\tau = \tau_p + \tau_r + \tau_b + \tau_i$, are displayed as a function of the strain ϵ for the simulation with $N = 2.2\times10^6$ atoms. All results were derived with a cut-off $q_c = 0.3$ Å^{-1}. Lines are guides to the eye.

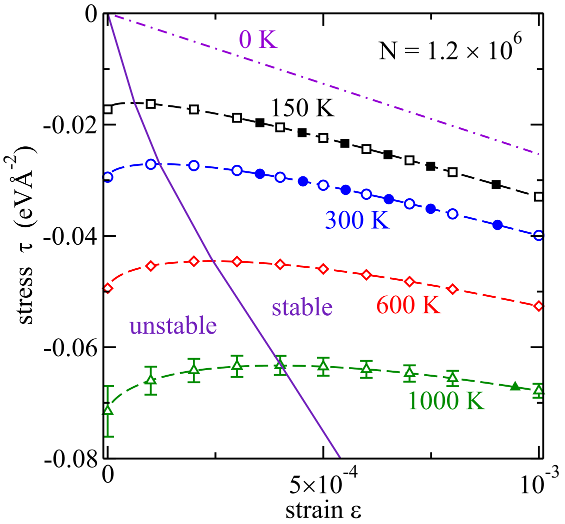

FIG. 9. Isothermal stress-strain curves as derived from $N\epsilon T$ simulations of a membrane with 1.2×10^6 atoms. The continuous line is the locus of critical points [maxima of the $\tau(\epsilon)$ curves]. This line is the boundary between thermodynamic stable and unstable regions of a crystalline membrane described by the Nelson-Peliti Hamiltonian. The filled symbols correspond to state points derived in the $N\tau T$ ensemble, as a check of the internal consistency of our simulations. The bars at 1000 K display the equilibrium root mean-squared fluctuation of the stress, $\sigma_\tau = (\langle\tau^2\rangle - \langle\tau\rangle^2)^{1/2}$, as derived in the canonical $N\epsilon T$ ensemble. The total bar length corresponds to the value $6\sigma_\tau$. The dashed lines are guides to the eye. All results were derived with a cut-off $q_c = 0.3$ Å^{-1}.

$\tau < 0$. In Fig. 8(b), the various contributions to the stress τ are displayed for the membrane with $N = 2.2\times10^6$ atoms. The most important contributions to the total stress τ are the terms τ_p and τ_r. The first one, τ_p depends on the strain of the projected area S_p [see Eq. (24)]. The second, τ_r depends on the additional strain caused by the excess area [see Eq. (25)]. The other two contributions to the stress, $\tau_b + \tau_i$, are comparatively small, and nearly independent of the strain ϵ.

Finite-size effects in the isothermal stress-strain curves of Fig. 8(a) are small. They are only noticeable when the strain vanishes, $\epsilon = 0$. In this case, the tensile stress τ becomes more negative as the size of the membrane increases.

The slopes of the curves $\tau_p(\epsilon)$ and $\tau_r(\epsilon)$ in Fig. 8(b) have opposite signs. The slope $\partial\tau_p/\partial\epsilon$ is a negative constant $(-2B_0)$ to first order in ϵ. However, the slope $\partial\tau_r/\partial\epsilon$ is always positive and decreases monotonically as ϵ increases. Figure 8(b) shows that when $\epsilon = 0$, the slope $\partial\tau_r/\partial\epsilon > |\partial\tau_p/\partial\epsilon|$. The larger the strain ϵ, the smaller the slope $\partial\tau_r/\partial\epsilon$, so that at a critical strain $\epsilon_c = 4\times10^{-4}$ both slopes become identical in absolute value but with opposite signs, i.e., $\partial\tau_r/\partial\epsilon = -\partial\tau_p/\partial\epsilon$. The critical point $\tau_c(\epsilon_c)$ corresponds to the maximum of the stress-strain curve in Fig. 8(a). At 1000 K the critical strain is $\epsilon_c = 4\times10^{-4}$.

The stability condition for the Helmholtz free energy $F(T, \epsilon, N)$ implies the convexity of the energy surface. The local condition for convexity is

$$\left(\frac{\partial^2 F}{\partial S_p^2}\right)_{N,T} = -\left(\frac{\partial\tau}{\partial S_p}\right)_{N,T} = \frac{1}{2LL_0}\left(-\frac{\partial\tau}{\partial\epsilon}\right)_{N,T} \geqslant 0\,. \quad (43)$$

Thus, a negative slope $\partial\tau/\partial\epsilon \leqslant 0$ is a necessary condition for thermodynamic stability. The state points in the isothermal curve of Fig. 8(a) are unstable for strains ϵ smaller than the critical value, $0 \leqslant \epsilon < \epsilon_c$. The most striking consequence of this is that a flat unstrained membrane with $\epsilon = 0$ is thermodynamically unstable at finite temperature.

The stability of the flat membrane is tied to a positive strain $\epsilon > \epsilon_c$, high enough to prevent the interaction energy $E_{i,\mathbf{q}}$ from being the dominant term in whatever range of q. This behavior is seen in Fig. 2. The flat membrane is unstable at 1000 K for the strains $\epsilon = 0$ [see Fig. 2(c)] and $\epsilon = 10^{-5}$ [see Fig. 2(b)]. Here the average interaction energy $\langle E_{i,\mathbf{q}}\rangle$ is seen to be the dominant energy in a region at low q. However, as the critical strain increases to the value $\epsilon_c = 4\times10^{-4}$ [see Fig. 2(a)], then the interaction energy $\langle E_{i,\mathbf{q}}\rangle$ becomes smaller than its competing energy terms, i.e., the bending $\langle E_{b,\mathbf{q}}\rangle$ or the excess area $\langle E_{r,\mathbf{q}}\rangle$ contributions, in the whole q range.

G. Stability region

Isothermal stress-strain curves of the membrane are displayed in Fig. 9 at several temperatures between 0 and 1000 K. The results were derived by $N\epsilon T$ simulations with $N = 1.2\times10^6$ atoms and a cut-off $q_c = 0.3$ Å^{-1}. The isotherm in the limit $T \to 0$ is simply $\tau \equiv \tau_p = -2B_0\epsilon$ (to first order in ϵ), as the amplitudes $A_\mathbf{q} \equiv 0$ in this limit. The continuous line approximates the locus of critical points (ϵ_c, τ_c), defined by the maximum of each isotherm. This line marks the boundary of the stable region of the flat membrane in the $\tau - \epsilon$ diagram. The critical strain ϵ_c is a monotonically increasing function of the temperature. The higher the temperature, the larger the tensile strain ϵ required for the flat membrane to reach its stability region where $\epsilon \geqslant \epsilon_c$.

An unstrained membrane ($\epsilon = 0$) is stable only in the limit $T \to 0$, where the stress $\tau = 0$. An increase in temperature causes tensile tension ($\tau \simeq \tau_r$), as thermal fluctuations increase the real area of the membrane. The stability condition of the Helmholtz free energy is violated when $\epsilon = 0$, as

$$\left(\frac{\partial \tau}{\partial \epsilon}\right)_{\epsilon=0} > 0\,, \tag{44}$$

because [see Fig. 8(b)]

$$\left(\frac{\partial \tau_r}{\partial \epsilon}\right)_{\epsilon=0} > -\left(\frac{\partial \tau_p}{\partial \epsilon}\right)_{\epsilon=0} = 2B_0\,. \tag{45}$$

The constraint of fixed projected area in the $N\epsilon T$ ensemble renders possible to perform MC simulations in regions where the flat membrane is thermodynamically unstable, provided that the state points are close enough to the stability region and display positive strain values, $\epsilon \geqslant 0$. This does not hold true for simulations in the constant stress ensemble $N\tau T$, where the projected area fluctuates. $N\tau T$ simulations are only possible in the stable region. State points derived from $N\tau T$ simulations at 150, 300, and 1000 K are displayed in Fig. 9 by filled symbols. We find that $N\tau T$ simulations in the stable region, but close to the critical point $\tau_c(\epsilon_c)$ may be driven into unstable trajectories. Unstable trajectories are characterized by unphysical large values of the out-of-plane amplitudes $A_{\mathbf{q}}$, unphysical large values of the real area S_r, as well as by a negative value of the strain ϵ of the membrane. In other words, the flat morphology of the membrane is not stable. The Nelson-Peliti Hamiltonian is an elastic model for the planar morphology of a crystalline membrane. Therefore, apart from the determination of the region of thermodynamic stability of the flat membrane, no further characterization of the membrane morphology in the unstable region can be derived from this Hamiltonian. This result has been unnoticed in previous studies using the Nelson-Peliti Hamiltonian [1,7,9,12,17].

Figure 9 shows that an unstrained flat membrane ($\epsilon = 0$) is unstable at any finite temperature. Therefore, when $\epsilon = 0$, the anomalous spectrum of out-of-plane fluctuations, defined with a critical exponent $\eta = 0.8$, corresponds to a model of a planar membrane that is thermodynamically unstable when described with the Nelson-Peliti Hamiltonian. Thus, the generally accepted view that the planar morphology of graphene and other 2D solid membranes is a consequence of displaying such an anomalous spectrum of out-of-plane fluctuations, is not supported by our simulations.

The strain-stress curves in Fig. 9 imply that by heating the solid membrane at constant stress, i.e., as the state point is moved along a horizontal line from the right to the left of Fig. 9, then the membrane will cross the critical line separating stable and unstable regions. Therefore, the Nelson-Peliti Hamiltonian predicts that the high temperature morphology of the solid membrane is not planar, but crumpled. This expectation is opposite to the behavior found in graphene simulations with realistic interatomic potentials. When a graphene layer is heated at a constant compressive stress, the morphology of the membrane changes from crumpled to planar as the temperature increases [28]. This behavior of a graphene layer with rising temperature signals the presence of additional anharmonic effects that are not included in the Nelson-Peliti Hamiltonian [29,30].

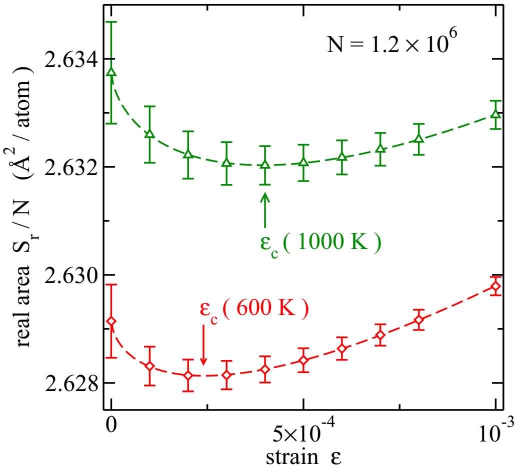

FIG. 10. Real area as a function of the strain ϵ, as derived from $N\epsilon T$ simulations of a membrane with 1.2×10^6 atoms. The isotherms at 600 and 1000 K are shown. The critical strain (ϵ_c) corresponds to the minimum value of the real area at a given temperature. The bars display the equilibrium root mean-squared fluctuation of the real area, $\sigma_{S_r/N} = (\langle S_r^2\rangle - \langle S_r\rangle^2)^{1/2}/N$, as derived in the canonical $N\epsilon T$ ensemble. The total bar length corresponds to the value $6\sigma_{S_r/N}$. All results were derived with a cut-off $q_c = 0.3$ Å^{-1}. The dashed lines are guides to the eye.

H. Real area and membrane stability

The state points along the critical line (ϵ_c, τ_c) in Fig. 9 display an interesting property related to the real area S_r of the membrane. At any given temperature the real area of the membrane takes its minimum value at the critical strain ϵ_c. This behavior is displayed in Fig. 10, where the real area is represented as a function of the strain at 600 and 1000 K, respectively. Along the displayed isotherms, only the state points with strain $\epsilon > \epsilon_c$ are thermodynamically stable.

The stress and the real area display a simple relationship. The real area in Eq. (20) can be expressed to first order in ϵ as

$$S_r = S_0(1 + 2\epsilon + \epsilon_r)\,, \tag{46}$$

where S_0 is the projected area when $\epsilon = 0$ (i.e., $S_0 = L_0^2$), and

$$\epsilon_r = \sum_{\mathbf{q}}^{BZ} \frac{q^2 |A_{\mathbf{q}}|^2}{2}\,. \tag{47}$$

The stress in Eq. (23) can be approximated as

$$\tau = -B_0(2\epsilon + \epsilon_r)\,. \tag{48}$$

In this equation, the contribution of the stress terms $\tau_b + \tau_i$ is neglected, as they are small [see Fig. 8(b)]; the term τ_p is approximated by its first order in ϵ; and in the term τ_r the strain ϵ was neglected in comparison to 1 [see Eq. (25)]. Combining Eqs. (46) and (48), one gets a linear dependence between stress and the real area of the crystalline membrane,

$$\tau = B_0 - \frac{B_0}{S_0} S_r\,. \tag{49}$$

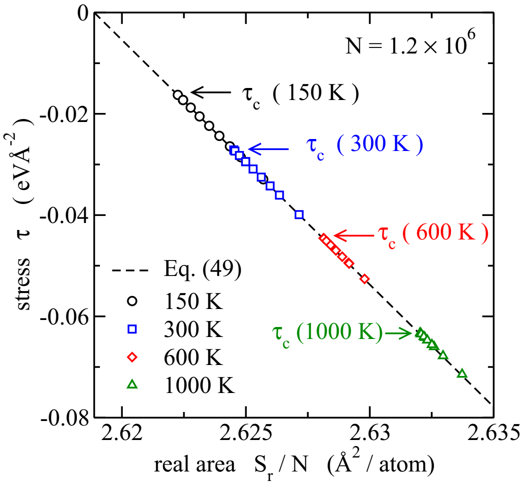

FIG. 11. Stress-real area isotherms as derived from $N\epsilon T$ simulations of a crystalline membrane with 1.2×10^6 atoms. The dashed line corresponds to Eq. (49). The state point with the minimum real area of each isotherm corresponds to the critical point $\tau_c(T)$. All results were derived with a cut-off $q_c = 0.3$ Å^{-1}.

The stress-strain isotherms previously shown in Fig. 9 are represented in Fig. 11 as isotherms in the plane stress-real area. The four isotherms appear as segments on a straight line given by Eq. (49), which is shown as a dashed line. Each of these isotherms includes both the thermodynamic stable and unstable points already analyzed in Fig. 9. One observes that all state points lie on the same straight line. For each isotherm, the state point with minimum real area corresponds to the critical point.

I. Anharmonic effects and membrane stability

Our MC simulations with the Nelson-Peliti Hamiltonian of an unstrained membrane ($\epsilon = 0$) successfully reproduce, for a large set of membrane sizes and temperatures, the predicted anomalous low-q behavior of the mean-square amplitudes, given by $\langle|A_q|^2\rangle \propto q^{\eta-4}$ with a critical exponent $\eta \sim 0.8$. This result demonstrates excellent agreement with SCSA and RG methods, as well as with previous simulation results [see Figs. 3(a) and 6(a)] [8–14]. By applying a weak strain $0 < \epsilon \ll 1$ to the membrane, the strict low-q limit of $\langle|A_q|^2\rangle$ changes to a regular q^{-2} behavior. Our simulations with $\epsilon > 0$ reveal that the anomalous low-q limit, characterized by a precise critical value of η, can still be accurately determined through the analysis of $\langle|A_q|^2\rangle$ across a wide range of intermediate q values, and a subsequent extrapolation of the results to the $\epsilon = 0$ limit [see Fig. 5(c)]. Therefore, our findings reaffirm the established view that the Nelson-Peliti Hamiltonian captures the essential anharmonic effects on the out-of-plane fluctuations due to the approximate treatment of the in-plane fluctuations in the graphene layer.

However, our analysis of the strain-stress curves associated to the Nelson-Peliti Hamiltonian shows a systematic issue that, to our knowledge, has not been previously reported [see Figs. 8(a) and 9]. A membrane described by this Hamiltonian becomes mechanically unstable at finite temperature over a range of strains, $\epsilon \geqslant 0$, that spans the entire region used for extrapolating the anomalous low-q behavior. This result contrasts with the stability of the flat morphology of graphene found in simulations with atomistic carbon potentials [17,28,31]. The mechanical instability arises from the approximation used in the Hamiltonian to incorporate in-plane fluctuations as anharmonic contributions to the out-of-plane fluctuations. The primary goal of the Nelson-Peliti Hamiltonian has never been to accurately describe a graphene sheet but rather to offer the simplest RG analysis for understanding the anomalous behavior of the fluctuating membrane. Therefore, one might expect that the mechanical stability of the Hamiltonian model could be achieved, without changing its relevant scaling properties, by some tuning of the model parameters or by the addition of some regular contribution to the Hamiltonian.

To search for a mechanically stable version of the Nelson-Peliti Hamiltonian, we first explore the role of the cut-off q_c in the sums over the BZ that appear in the elastic model. This cut-off is largely undefined in any RG model Hamiltonian and most of our simulations were carried out with $q_c = 0.3$ Å^{-1}, quite below the limit of the BZ in graphene ($q_c = 1.3$ Å^{-1}). Then, we are leaving out a large contribution to the anharmonic term of the Hamiltonian.

To assess how the results in Figs. 9–11 are affected by the employed cut-off, a new set of $N\epsilon T$ simulations was performed by varying q_c in the interval $0.05 \leqslant q_c \leqslant 1.3$ Å^{-1}. The effect of changing q_c is displayed in Fig. 12(a) for the stress-strain isotherm, in Fig. 12(b) for the real area-strain curve, and in Fig. 12(c) for the stress-real area graph. These results correspond to a temperature of 1000 K and a membrane size of $N = 1.3\times10^5$ atoms. The results in Fig. 12(a) for $0.3 < q_c \leqslant 1.3$ Å^{-1} show that increasing q_c produces a shift of the stress-strain curves with a very slight, hardly noticeable increase of the range of instability. This small effect does not change our conclusions in connection with Figs. 9–11.

Interestingly, increased stability must be sought in the opposite direction, by reducing the value of q_c, thus avoiding the inclusion of anharmonic contributions for large values of q. As observed in the stress-strain curves of Fig. 12(a), the range of mechanical instability can be narrowed from $\epsilon \lesssim 4\times10^{-4}$ for $q_c = 1.3$ Å^{-1} to approximately $\epsilon \lesssim 3\times10^{-4}$ for $q_c = 0.1$ Å^{-1}, and further to $\epsilon \lesssim 10^{-4}$ for $q_c = 0.05$ Å^{-1}. Thus, reducing anharmonic effects in the Nelson-Peliti Hamiltonian by lowering the value of the cut-off q_c indeed makes it stable for lower values of the strain ϵ.

The square amplitudes $\langle|A_{\mathbf{q}}|^2\rangle$ for the unstrained membrane ($\epsilon = 0$), previously displayed in Fig. 3(a), allowed us to accurately fit the exponent $\eta \sim 0.8$ over more than two orders of magnitude for q. In Fig. 12(d), the square amplitudes $\langle|A_{\mathbf{q}}|^2\rangle$ are represented for $\epsilon = 0$ for a fixed system size and varying cut-off values. As the cut-off is reduced, the range of low-q values exhibiting nonanalytical behavior in the out-of-plane fluctuations also decreases. Further lowering of q_c leads to an enhancement of $\langle|A_{\mathbf{q}}|^2\rangle$ for $q \leqslant q_c$, which deviates from the $q^{\eta-4}$ behavior observed in the simulations with larger q_c. Thus, the instability of the model when $\epsilon = 0$ seems to be associated to the $q^{\eta-4}$ dependence of the out-of-plane amplitudes.

A second approach to achieving mechanical stability in the Nelson-Peliti Hamiltonian is to introduce an additional term

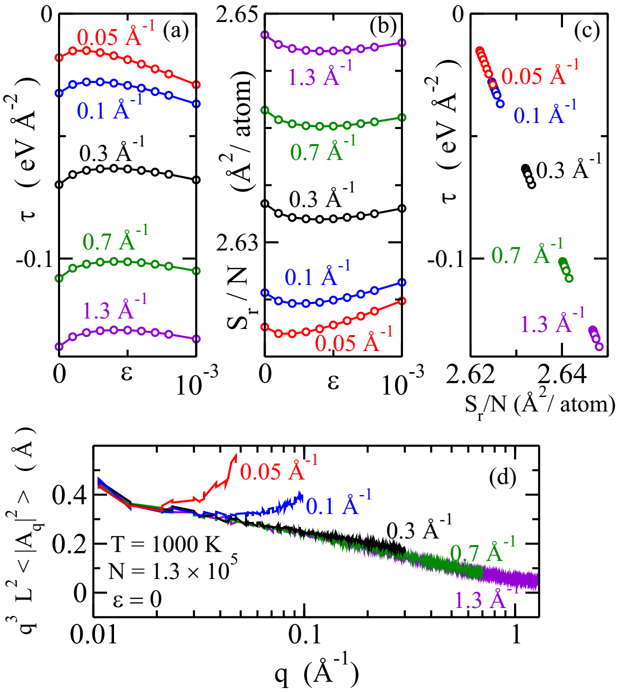

FIG. 12. Effect of the cut-off q_c on several isothermal properties derived by MC simulations of a membrane in the $N\epsilon T$ ensemble: (a) stress-strain curve; (b) real area-strain curve; and (c) stress-real area curve. In panel (d) the function $q^3L^2\langle|A_{\mathbf{q}}|^2\rangle$ is displayed as a function of q_c for the unstrained membrane ($\epsilon = 0$) and several values of q_c. The simulations correspond to membrane size of $N = 1.3\times10^5$ atoms at $T = 1000$ K. The cut-off q_c was varied between 0.05 and 1.3 Å^{-1}. The last value corresponds to the boundary of the BZ in graphene. The critical tensile strain ϵ_c corresponds to the maximum of the curves in panel (a) and the minimum in panel (b). ϵ_c becomes lower as the value of the cut-off employed in the simulations is reduced.

that would be irrelevant for the low-q renormalization analysis. The simplest choice is a higher-order dispersion term $\sim q^6$, achieved by adding a new elastic energy E_6 to the original Nelson-Peliti Hamiltonian of Eq. (13),

$$E_6 = \sum_{\mathbf{q}}^{BZ} L^2 K_6 q^6 |A_{\mathbf{q}}|^2 \,, \tag{50}$$

where K_6 is a positive constant with the dimension of energy×length^2. The isothermal stress-strain curves for a membrane with $N = 1.3\times10^5$ atoms at a temperature of 1000 K and $q_c = 0.3$ Å^{-1} are displayed in Fig. 13(a) for various values of the constant K_6. The corresponding square amplitudes $\langle|A_{\mathbf{q}}|^2\rangle$ are represented in Fig. 13(b). Increasing K_6 leads to a significant reduction in the amplitude of high-q out-of-plane fluctuations, consequently weakening their anharmonic contribution. Figure 13(a) shows that the range of mechanical stability increases with larger K_6. However, the largest value of $K_6 = 1.28\times10^4$eVÅ^2, used in Fig. 13 to achieve mechanical stability for $\epsilon \leqslant 10^{-4}$, is by far too large to provide a physical description of graphene. The bending $\langle E_b\rangle$ and interaction $\langle E_i\rangle$ energies amounts to only 0.4% and 0.2%, respectively, while nearly all the elastic energy (99.4%)

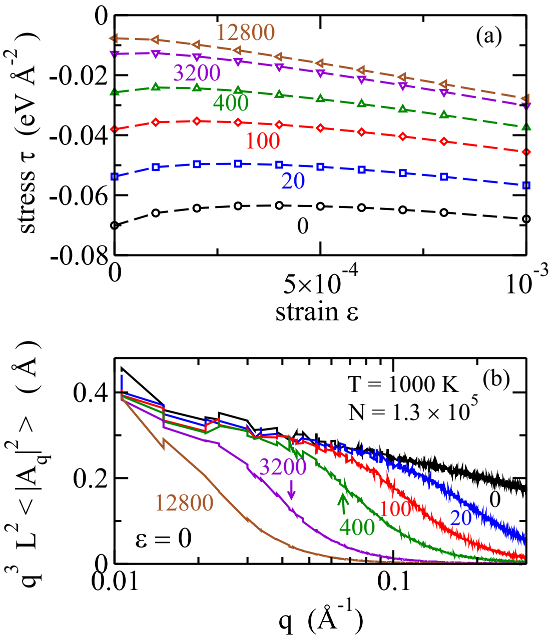

FIG. 13. (a) Isothermal stress-strain curves as derived from $N\epsilon T$ simulations of a membrane for different values of the coupling constant K_6 (in eVÅ^2). K_6 defines a q^6-dispersion term in Eq. (50) that has been added to the Nelson-Peliti Hamiltonian. The critical strain ϵ_c (maximum of the curve) is displaced towards $\epsilon = 0$ as the constant K_6 increases. Dashed lines are guides to the eye. (b) The function $q^3L^2\langle|A_{\mathbf{q}}|^2\rangle$ is plotted against q, for several values of the constant K_6, in the case of an unstrained membrane ($\epsilon = 0$). All results were derived with $N = 1.3\times10^5$ atoms at 1000 K and using a cut-off $q_c = 0.3$ Å^{-1}.

corresponds to the average $\langle E_6\rangle$. Even more relevant is that, as shown in Fig. 13(b), the range of q over which the anomalous q behavior is observed is strongly reduced due to the damping effect of the E_6 term on the amplitude $\langle|A_{\mathbf{q}}|^2\rangle$ at large q, which in turn reduces the anharmonic effects of the model. We have confirmed that increasing the cut-off value, q_c, from 0.3 to 1.3 Å^{-1} in the stress-strain curves depicted in Fig. 13(a) yields an effect similar to that shown in Fig. 12(a). The $\tau(\epsilon)$ curves are rigidly shifted as q_c increases, without any significant change in the slopes of the curves.

The strong and accurate evidence for the anomalous behavior observed in our simulations, in excellent agreement with the RG analysis of the Nelson-Peliti Hamiltonian, fully disappears when we try to ensure the mechanical stability of the model. We cannot discard that with membranes of huge sizes, beyond the scope of simulation studies, there might be a range of very low-q values where the goals of mechanical stability at $\epsilon = 0$ and the observation of the RG prediction for $\eta = 0.8$ could be made compatible through appropriate choices of q_c, K_6, or adding some other regular terms to the original Nelson-Peliti Hamiltonian. However, based on the extensive evidence from our simulations, we are inclined to accept the alternative possibility that these two goals are fundamentally incompatible. In other words, the same anharmonic effects that are included in an approximated, truncated manner in the Nelson-Peliti Hamiltonian, and are the source

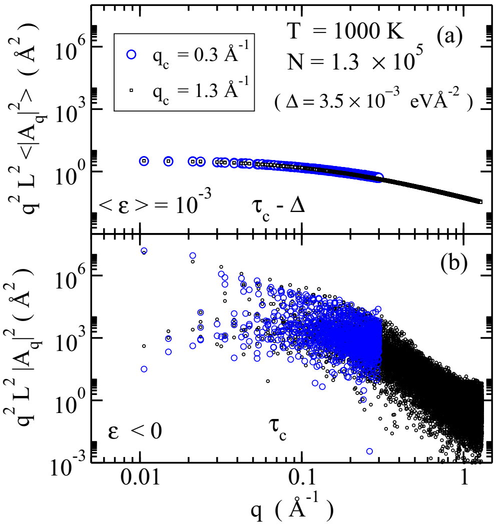

FIG. 14. Square amplitudes of the out-of-plane modes of a crystalline layer are derived in the $N\tau T$ ensemble at the critical stress τ_c [corresponding to the maximum of the $\tau(\epsilon)$ curve] and at a stable state point defined at a higher tensile stress. These simulations were performed at a temperature of $T = 1000$ K with $N = 1.3\times10^5$ atoms, employing two different cut-off values: $q_c = 0.3$ and 1.3 Å^{-1}. (a) The average square amplitudes are presented as $q^2L^2\langle|A_{\mathbf{q}}|^2\rangle$ as a function of q for a stress, $\tau_c - \Delta$, where $\Delta = 3.5\times10^{-3}$ eVÅ^{-2}, corresponding to a thermodynamically stable state point. (b) The instantaneous square amplitudes are shown at the critical stress τ_c after a simulation run of 5×10^3 MCS. Notably, the violent fluctuations of the out-of-plane amplitudes in panel (b) are independent of the size of the cut-off.

of the anomalous behavior predicted by the RG analysis, are also responsible for its mechanical instability.

In finite-size systems governed by long-range interactions, the convexity in the Helmholtz free energy may not be strictly necessary for thermal stability. This is because surface and interface contributions may become significant compared to bulk contributions [32]. In the context of our simulations of a crystalline membrane with the Nelson-Peliti Hamiltonian, it is important to emphasize that the evidence of the thermal instability is not solely indicated by the positive slopes of the $\tau(\epsilon)$ curves. It is also evident in the violent out-of-plane fluctuations observed at constant stress simulations.

This behavior is illustrated in Fig. 14, where the square amplitudes of the out-of-plane modes are studied in the $N\tau T$ ensemble. We conducted simulations at the critical stress τ_c and at a slightly higher tensile stress, $\tau_c - \Delta$, with $\Delta = 3.5\times10^{-3}$ eVÅ^{-2}. The latter stress corresponds to a state point in the thermodynamically stable region. The average out-of-plane amplitudes at this stable state point are depicted in Fig. 14(a). The results obtained with the cut-offs $q_c = 0.3$ and 1.3 Å^{-1} display excellent agreement. In this constant stress simulations at $\tau_c - \Delta$, the projected area fluctuates with instantaneous values corresponding to positive strains, $\epsilon > 0$, centered around an ensemble average of $\langle\epsilon\rangle = 10^{-3}$.

At the critical tension τ_c, the out-of-plane amplitudes exhibit a monotonous increase throughout the simulation run, a manifestation of the thermodynamic instability in the constant stress trajectory. Consequently, in Fig. 14(b), we present the instantaneous amplitudes obtained after a simulation run with 5×10^3 MCS. It is noteworthy that, in stark contrast to the average amplitudes found at the stable state point, the instantaneous out-of-plane amplitudes at τ_c fluctuate over more than seven orders of magnitude.

Furthermore, we observe that these violent out-of-plane fluctuations persist regardless of the chosen cut-off value, whether it is $q_c = 0.3$ or 1.3 Å^{-1}. Unstable constant stress $N\tau_cT$ trajectories, characterized by a monotonous increase in out-of-plane amplitudes during the simulation run, are associated with a continuous drift in the instantaneous value of the membrane's projected area, resulting in a negative strain value, $\epsilon < 0$. Consequently, in constant stress simulations, when the flat morphology of the membrane is unstable, the projected area exhibits a monotonous decrease along the simulation rather than fluctuating around an average value, as observed in stable equilibrium conditions. The huge values and fluctuations in the instantaneous amplitudes under these unstable conditions should be interpreted as outcomes of the simulation trajectory, rather than as representative of a stable equilibrium.

The apparent contradiction between the stability observed in atomistic simulations of graphene [17,28] and the instability identified in the elastic Nelson-Peliti model could potentially be resolved through the following consideration. The coupling to an external tensile strain adds a q^2 term to the $\rho\omega_q^2$ dispersion of the flexural modes of a flat layer [17,27,33], which stabilizes its planar morphology. Similarly, any intrinsic anharmonic coupling causing a q^2 dispersion of the out-of-plane modes should also contribute to the layer's stability. Interestingly, various independent studies have demonstrated that intrinsic anharmonic effects induce a q^2 dispersion of the flexural modes of graphene. For example, Michel *et al.*, using a Hamiltonian with anharmonic terms of third and fourth order in lattice displacements, report an anharmonic renormalization of the flexural mode with a q^2 dispersion [34,35]. This result was also obtained within a continuum theory of crystalline membranes incorporating cubic interactions between in-plane and out-of-plane modes [5]. Adamyan *et al.* show, by an adiabatic approximation, that adding quadratic terms of the type $(\partial_i u_j)(\partial_j u_i)$ in the definition of the in-plane strain in Eq. (3) results in flexural phonon modes acquiring a q^2 dispersion [29]. It appears that the significance of these findings has not received enough attention by the graphene community, which has favored a model based on a critical exponent η to explain the stability of the flat morphology of unstrained crystalline membranes. Our MC simulations challenge the prevailing physical relevance attributed to the critical exponent model.

V. SUMMARY

A MC study of a crystalline membrane described by the Nelson-Peliti Hamiltonian has been presented using a set of elastic constants appropriate to graphene. All the simulations are performed in the classical limit, i.e., quantum effects that may appear at low temperatures are neglected in this paper. The membrane is studied subjected to a tensile biaxial strain $\epsilon \geqslant 0$.

For the case of an unstrained membrane ($\epsilon = 0$), our MC simulations are in good agreement with previous simulations based on the same Hamiltonian [13,14], and also with analytical results of the SCSA and RG methods [9,12]. In particular, the spectrum of out-of-plane fluctuations of an unstrained membrane in the long-wavelength limit displays a dependence $|A_q|^2 \propto q^{\eta-4}$, with a value of the critical exponent $\eta = 0.80 \pm 0.01$. This q dependence changes in the presence of a finite positive biaxial strain $\epsilon > 0$ to $|A_q|^2 \propto q^{-2}$, in good agreement with previous numerical simulations and analytic approximations [6,17].

Interesting results are derived from the isotherms in a strain-stress plane of the membrane described by the Nelson-Peliti Hamiltonian. The isotherms show that the stability of the flat membrane is tied to a positive biaxial strain $\epsilon > \epsilon_c$ larger than a critical value. ϵ_c must be high enough to prevent the interaction energy $E_{i,\mathbf{q}}$ from being the dominant factor in whatever range of q. This positive critical strain ϵ_c increases monotonically with temperature. By increasing the temperature at a constant tensile biaxial stress, the planar morphology of the membrane becomes unstable and the membrane crumples at high temperatures. The unstrained flat membrane ($\epsilon = 0$) is thermodynamically unstable at any finite temperature.

The instability of the planar morphology is also related to the dependence of the real area of the membrane with the strain at isothermal conditions. The real area is a quantitative measure of the square amplitude of the out-of-plane fluctuations divided by the square of their wavelength. In the planar morphology, the real area decreases as the biaxial tensile strain decreases, until the critical strain ϵ_c is reached. By a further decrease of the strain, with $\epsilon < \epsilon_c$, the real area increases, and the stable morphology of the membrane becomes crumpled.

Although anharmonic effects described by the Nelson-Peliti Hamiltonian imply a drastic reduction of the amplitude of the out-of-plane fluctuations, in comparison to the harmonic limit of the bending energy, this reduction is not large enough to stabilize the planar morphology of the unstrained ($\epsilon = 0$) membrane at finite temperatures. All the state points where the planar crystalline membrane is stable, display a long-wavelength dependence of the out-of-plane modes that varies as $|A_q|^2 \propto q^{-2}$.

Our results are significant for the present understanding of the anharmonic effects that are responsible for the stability of the planar morphology of solid membranes, like graphene. The generally accepted picture that the spectrum of out-of-plane fluctuations of unstrained graphene membrane has a dependence $|A_q|^2 \propto q^{\eta-4}$, with a critical exponent $\eta \sim 0.8$ in the long-wavelength limit, is not supported by our simulations. The prediction with this Hamiltonian is that a crystalline membrane with such a spectrum of out-of-plane fluctuations should be crumpled. Moreover, the Nelson-Peliti Hamiltonian predicts that the high-temperature morphology of a crystalline membrane is crumpled. However, previous simulations of graphene with atomistic interatomic potentials show that a planar morphology is favored at high temperatures, in comparison to a crumpled one [28]. Our final conclusion is that a crystalline membrane, like graphene, display significant anharmonic effects in addition to those already included in the Nelson-Peliti Hamiltonian.

ACKNOWLEDGMENTS

This work was supported by the Ministerio de Ciencia e Innovación (Spain) through Grant No. PID2022-139776NB-C66 and Grant No. PID2020-117080RB and from the Maria de Maeztu Programme for Units of Excellence in R&D (Grant No. CEX2018-000805-M).

APPENDIX: GAUSSIAN CURVATURE

The function $C_{ij}(\mathbf{q})$ in Eq. (19) is the Fourier transform of a product of real space functions [6],

$$C_{ij}(\mathbf{q}) = \mathbb{F}_{\mathbf{q}}[\partial_i z(\mathbf{r})\partial_j z(\mathbf{r})]. \tag{A1}$$

From the inverse Fourier transform of this relation and with the definition of $\Psi(\mathbf{q})$ in Eq. (18), one derives after some algebra

$$q^2\Psi(\mathbf{q}) = \mathbb{F}_{\mathbf{q}}[2G(\mathbf{r})]\,, \tag{A2}$$

where $G(\mathbf{r})$ is the Gaussian curvature,

$$G(\mathbf{r}) = \partial^2_{xx}z(\mathbf{r})\partial^2_{yy}z(\mathbf{r}) - \left[\partial^2_{xy}z(\mathbf{r})\right]^2 . \tag{A3}$$

If we define the function $g(\mathbf{r})$ as that one whose mean curvature is equal to minus two times the Gaussian curvature, namely,

$$2G(\mathbf{r}) = -\left(\partial^2_{xx}g(\mathbf{r}) + \partial^2_{yy}g(\mathbf{r})\right) = -\nabla^2 g(\mathbf{r})\,, \tag{A4}$$

then by taking the Fourier transform of this expression and comparing the result to Eq. (A2), one derives

$$\Psi(\mathbf{q}) = \mathbb{F}_{\mathbf{q}}[g(\mathbf{r})]\,. \tag{A5}$$

The Parseval theorem implies that

$$\sum_{\mathbf{q}}^{BZ} |\Psi(\mathbf{q})|^2 = \frac{1}{L^2}\int_0^L\int_0^L dxdy\, g(\mathbf{r})^2\,. \tag{A6}$$

The right-hand side of the last equation was the form chosen by Nelson and Peliti to express the interaction energy E_i of Eq. (17). The function $g(\mathbf{r})$ in Eq. (A4) can be written as [1]

$$g(\mathbf{r}) = -2(\nabla^2)^{-1}G(\mathbf{r}) = P^T_{ij}\,\partial_i z\partial_j z\,, \tag{A7}$$

where P^T_{ij} is the transverse operator

$$P^T_{ij} = (\nabla^2)^{-1}\varepsilon_{ik}\varepsilon_{jl}\partial_k\partial_l\,. \tag{A8}$$

The sum over repeated indices is implicit, and ε_{ik} is the Levi-Civita symbol ($\varepsilon_{ii} = 0,\ \varepsilon_{12} = 1, \varepsilon_{21} = -1$).

---

[1] D. R. Nelson and L. Peliti, Fluctuations in membranes with crystalline and hexatic order, J. Phys. France **48**, 1085 (1987).

[2] J. A. Aronovitz and T. C. Lubensky, Fluctuations of solid membranes, Phys. Rev. Lett. **60**, 2634 (1988).

[3] F. Ahmadpoor and P. Sharma, A perspective on the statistical mechanics of 2D materials, Extreme Mech. Lett. **14**, 38 (2017).

[4] B. Amorim, A. Cortijo, F. de Juan, A. G. Grushin, F. Guinea, A. Gutiérrez-Rubio, H. Ochoa, V. Parente, R. Roldán, P. San-Jose, J. Schiefele, M. Sturla, and M. A. H. Vozmediano, Novel effects of strains in graphene and other two dimensional materials, Phys. Rep. **617**, 1 (2016).

[5] B. Amorim, R. Roldán, E. Cappelluti, A. Fasolino, F. Guinea, and M. I. Katsnelson, Thermodynamics of quantum crystalline membranes, Phys. Rev. B **89**, 224307 (2014).

[6] F. Ahmadpoor, P. Wang, R. Huang, and P. Sharma, Thermal fluctuations and effective bending stiffness of elastic thin sheets and graphene: A nonlinear analysis, J. Mech. Phys. Solids **107**, 294 (2017).

[7] O. Coquand and D. Mouhanna, Flat phase of quantum polymerized membranes, Phys. Rev. E **94**, 032125 (2016).

[8] P. Le Doussal and L. Radzihovsky, Self-consistent theory of polymerized membranes, Phys. Rev. Lett. **69**, 1209 (1992).

[9] P. Le Doussal and L. Radzihovsky, Anomalous elasticity, fluctuations and disorder in elastic membranes, Ann. Phys. **392**, 340 (2018).

[10] J.-P. Kownacki and D. Mouhanna, Crumpling transition and flat phase of polymerized phantom membranes, Phys. Rev. E **79**, 040101(R) (2009).

[11] F. L. Braghin and N. Hasselmann, Thermal fluctuations of free-standing graphene, Phys. Rev. B **82**, 035407 (2010).

[12] A. Mauri and M. I. Katsnelson, Scaling behavior of crystalline membranes: An ϵ-expansion approach, Nucl. Phys. B **956**, 115040 (2020).

[13] A. Tröster, High-precision fourier Monte Carlo simulation of crystalline membranes, Phys. Rev. B **87**, 104112 (2013).

[14] A. Tröster, Fourier Monte Carlo simulation of crystalline membranes in the flat phase, J. Phys.: Conf. Ser. **454**, 012032 (2013).

[15] J. H. Los, M. I. Katsnelson, O. V. Yazyev, K. V. Zakharchenko, and A. Fasolino, Scaling properties of flexible membranes from atomistic simulations: Application to graphene, Phys. Rev. B **80**, 121405(R) (2009).

[16] J. Hašík, E. Tosatti, and R. Martoňák, Quantum and classical ripples in graphene, Phys. Rev. B **97**, 140301(R) (2018).

[17] R. Roldán, A. Fasolino, K. V. Zakharchenko, and M. I. Katsnelson, Suppression of anharmonicities in crystalline membranes by external strain, Phys. Rev. B **83**, 174104 (2011).

[18] W. Gao and R. Huang, Thermomechanics of monolayer graphene: Rippling, thermal expansion and elasticity, J. Mech. Phys. Solids **66**, 42 (2014).

[19] F. Behroozi, Theory of elasticity in two dimensions and its application to Langmuir-Blodgett films, Langmuir **12**, 2289 (1996).

[20] E. Chacón, P. Tarazona, and F. Bresme, A computer simulation approach to quantify the true area and true area compressibility modulus of biological membranes, J. Chem. Phys. **143**, 034706 (2015).

[21] C. P. Herrero and R. Ramírez, Thermodynamic properties of graphene bilayers, Phys. Rev. B **101**, 035405 (2020).

[22] R. J. T. Nicholl, H. J. Conley, N. V. Lavrik, I. Vlassiouk, Y. S. Puzyrev, V. P. Sreenivas, S. T. Pantelides, and K. I. Bolotin, The effect of intrinsic crumpling on the mechanics of free-standing graphene, Nat. Commun. **6**, 8789 (2015).

[23] R. J. T. Nicholl, N. V. Lavrik, I. Vlassiouk, B. R. Srijanto, and K. I. Bolotin, Hidden area and mechanical nonlinearities in freestanding graphene, Phys. Rev. Lett. **118**, 266101 (2017).

[24] R. C. Tolman, *Statistical Mechanics with Applications to Physics and Chemistry* (Chemical Catalog Co., New York, 1927).

[25] L. D. Landau and E. M. Lifshitz, *Statistical Physics*, 3rd ed. (Pergamon Press, Oxford, 1980).

[26] R. Ramírez and C. P. Herrero, Phonon dispersion in two-dimensional solids from atomic probability distributions, J. Chem. Phys. **151**, 224107 (2019).

[27] R. Ramírez and C. P. Herrero, Anharmonicity of the acoustic modes of graphene, Phys. Rev. B **101**, 235436 (2020).

[28] R. Ramírez and C. P. Herrero, Thermal control of graphene morphology: A signature of its intrinsic surface tension, Phys. Rev. B **97**, 235426 (2018).

[29] V. M. Adamyan, V. N. Bondarev, and V. V. Zavalniuk, Bending sound in graphene: Origin and manifestation, Phys. Lett. A **380**, 3732 (2016).

[30] V. N. Bondarev, V. M. Adamyan, and V. V. Zavalniuk, Bending mode and thermal expansion of graphene, Phys. Rev. B **97**, 035426 (2018).

[31] C. P. Herrero and R. Ramírez, Path-integral simulation of graphene monolayers under tensile stress, Phys. Chem. Chem. Phys. **19**, 31898 (2017).

[32] D. H. E. Gross, *Microcanonical Thermodynamics: Phase Transitions in 'Small' Systems* (World Scientific, Singapore, 2001).

[33] P. L. de Andres, F. Guinea, and M. I. Katsnelson, Bending modes, anharmonic effects, and thermal expansion coefficient in single-layer and multilayer graphene, Phys. Rev. B **86**, 144103 (2012).

[34] K. H. Michel, S. Costamagna, and F. M. Peeters, Theory of thermal expansion in 2D crystals, Phys. Status Solidi (b) **252**, 2433 (2015).

[35] K. H. Michel, S. Costamagna, and F. M. Peeters, Theory of anharmonic phonons in two-dimensional crystals, Phys. Rev. B **91**, 134302 (2015).

[36] J. H. Los, L. M. Ghiringhelli, E. J. Meijer, and A. Fasolino, Improved long-range reactive bond-order potential for carbon. I. Construction, Phys. Rev. B **72**, 214102 (2005).